# Decoupling of erosion and precipitation in the Himalayas

**D. W. Burbank[1], A. E. Blythe[2], J. Putkonen[3], B. Pratt-Sitaula[1], E. Gabet[1], M. Oskin[1], A. Barros[4] & T. P. Ojha[5]**

[1]*Department of Geological Sciences, University of California, Santa Barbara, California 93106, USA*
[2]*Department of Earth Sciences, University of Southern California, Los Angeles, California 90089, USA*
[3]*Department of Earth and Space Sciences, University of Washington, Seattle, Washington 98195, USA*
[4]*Division of Engineering and Applied Sciences, Harvard University, Cambridge, Massachusetts 02138, USA*
[5]*Himalayan Experience, 659-1 Mhepi, Kathmandu 3, Nepal*

**The hypothesis that abrupt spatial gradients in erosion can cause high strain rates in active orogens has been supported by numerical models that couple erosional processes with lithospheric deformation via gravitational feedbacks[1–3]. Most such models invoke a 'stream-power' rule, in which either increased discharge or steeper channel slopes cause higher erosion rates. Spatial variations in precipitation and slopes are therefore predicted to correlate with gradients in both erosion rates and crustal strain. Here we combine observations from a meteorological network across the Greater Himalaya, Nepal, along with estimates of erosion rates at geologic timescales (greater than 100,000 yr) from low-temperature thermochronometry. Across a zone of about 20 km length spanning the Himalayan crest and encompassing a more than fivefold difference in monsoon precipitation, significant spatial variations in geologic erosion rates are not detectable. Decreased rainfall is not balanced by steeper channels. Instead, additional factors that influence river incision rates, such as channel width and sediment concentrations, must compensate for decreasing precipitation. Overall, spatially constant erosion is a response to uniform, upward tectonic transport of Greater Himalayan rock above a crustal ramp.**

Contrasting styles of strain on the southern versus the northern flanks of the Tibetan plateau suggest potential responses to precipitation variations: within the narrow Himalayan belt, monsoon precipitation has removed mass and localized deformation since Miocene times[4], whereas ineffective erosion under drier climates has led to accretion and northward migration of deformation in northern Tibet[5]. Such interpretations of tectonic–precipitation linkages, as well as predictions of coupled geodynamic–erosion models, can only be tested against field data in situations where the measurable signals rise well above the noise of natural systems. The Nepalese Himalaya appear well suited for such a test, because they encompass abrupt gradients in precipitation, erosion and deformation.

The Marsyandi River catchment in the Annapurna Himalaya (Fig. 1) is one of the few drainages that cuts nearly orthogonal to Himalayan structural trends, and extends without major deviations from the southern edge of the Tibetan plateau to the Himalayan foreland. From its headwaters in Tibetan sedimentary strata, the Marsyandi crosses the South Tibetan fault (STF) system[4,6] before traversing the Greater Himalayan crystalline belt in a gorge incised between peaks rising to >7,000 m (Fig. 2a). On crossing the Main Central thrust (MCT), the Marsyandi flows through the Lesser Himalaya and crosses the Main Boundary Thrust (MBT) as it enters the Ganges basin. Both the STF system, a primarily down-to-the-north normal fault system, and the MCT, an up-to-the-south thrust fault, experienced major displacement in the early Miocene (~20–15 Myr ago)[4,6]. The MCT zone comprises both the classic MCT ('MCT I', Fig. 1), as well as a swath ~10 km wide ('MCT zone', Fig. 1) in the northernmost part of the MCT I footwall, where young cooling ages indicate accelerated Plio-Pleistocene erosion[7,8]. The likelihood of Quaternary displacement in the MCT zone and the STF system is currently debated[4,9,10].

A newly established meteorological network (Fig. 1) spans from

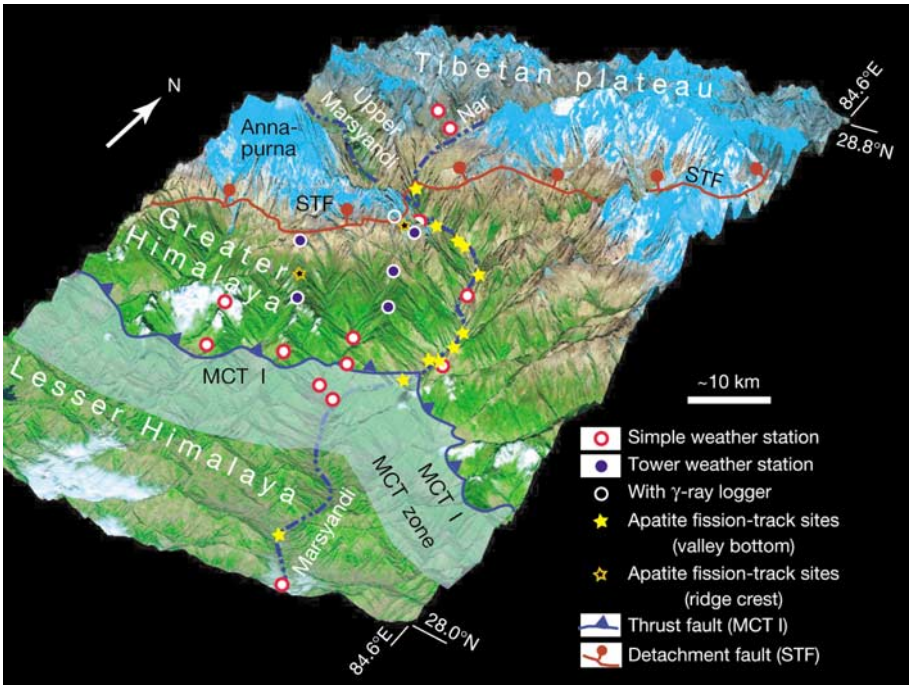


**Figure 1** Three-dimensional perspective view of study area, showing locations of major geologic structures, meteorological stations, and apatite fission-track samples. Sites with 10-m-tall weather towers or with γ-ray loggers are distinguished from 'simple' stations. Approximate traces of the MCT I and STF system are shown, along with the 'MCT zone' delineating the northern footwall of the MCT I.

Table 1 **Apatite fission-track ages in the Marsyandi catchment**

| Sample | Topographic position | Age (Myr) | 1σ (Myr) | Latitude, N | Longitude, E | Elevation |
|---|---|---|---|---|---|---|
| NBE-2 | Valley | 3.8 | 0.5 | 28° 01.473′ | 84° 27.500′ | 474 |
| NBE-4 | Valley | 1.9 | 1.1 | 28° 19.538′ | 84° 24.095′ | 900 |
| FT-JP-00-07 | Valley | 0.7 | 0.2 | 28° 23.242′ | 84° 24.173′ | 1,210 |
| NBE-5 | Valley | 0.4 | 0.2 | 28° 23.482′ | 84° 24.311′ | 1,100 |
| NBE-13 | Valley | 0.3 | 0.2 | 28° 25.334′ | 84° 24.115′ | 1,320 |
| NBE-11 | Valley | 0.5 | 0.2 | 28° 30.637′ | 84° 21.641′ | 1,850 |
| NBE-9 | Valley | 0.9 | 0.3 | 28° 31.763′ | 84° 20.615′ | 2,280 |
| FT-4-97 | Valley | 0.0 | 0.2 | 28° 31.800′ | 84° 19.253′ | 2,300 |
| NBE-10 | Valley | 0.5 | 0.2 | 28° 31.997′ | 84° 20.615′ | 2,150 |
| NBE-8a | Valley | 0.4 | 0.2 | 28° 33.683′ | 84° 15.640′ | 2,640 |
| FT-1-97 | Ridge crest | 1.2 | 0.3 | 28° 29.616′ | 84° 18.205′ | 4,100 |
| JP-FT-01-2 | Ridge crest | 0.8 | 0.2 | 28° 22.971′ | 84° 15.236′ | 3,831 |

500 to 1,500 m in the Lesser Himalaya, rises to 4,500 m in the Greater Himalaya, and includes one site at 4,200 m in the Tibetan zone. The 4-yr record (Fig. 2b) indicates that precipitation in the Annapurna Himalaya is dominated by monsoon rainfall: 80–98% of the annual total accumulates between May and October. Rainfall in the Lesser Himalaya averages ~1.6 m $yr^{-1}$, but abruptly increases as the monsoon impinges on the southern Greater Himalayan slopes, where maximum monsoon rainfall (~4.3 m) occurs at ~3,000 m elevation. Striking variations occur perpendicular to the range as monsoon precipitation systematically decreases northward to <0.5 m in the Tibetan realm (Fig. 2b).

Spatial variations in erosion rates across the Himalaya at geologic timescales were assessed using apatite fission-track dating on bedrock samples spanning 50 km along the Marsyandi River from the southern edge of the Tibetan zone to the northern margin of the Lesser Himalaya (Table 1). Apatite fission-track ages are commonly interpreted to indicate the elapsed time since cooling below the annealing isotherm. When cooling is rapid (≥100 °C $Myr^{-1}$), as is usual here, the effective annealing temperature is ~140 °C (ref. 11). If the depth of the annealing isotherm and the trajectory of rocks towards the surface are estimated, apatite fission-track ages can be converted into mean erosion rates[12,13]. Even without a three-dimensional thermal and kinematic model, cooling rates obtained from analogous topographic positions (river bottoms) can be compared as proxies for relative erosion rates.

The apatite fission-track dates show a striking pattern in the context of Himalayan topography and rainfall (Fig. 2c). At the southernmost site, a ~4-Myr age yields a cooling rate of ~30 °C $Myr^{-1}$ for the northern part of the Lesser Himalaya. Apatite fission-track ages become younger and cooling rates more rapid as the Greater Himalaya are approached. In the MCT hanging wall, apatite fission-track ages abruptly drop to ~0.5 Myr, indicating cooling rates nearly an order of magnitude faster than in the nearby Lesser Himalaya. Across the ~20 km separating the MCT from the STF, the apatite fission-track ages show no systematic trend, but instead fluctuate around a mean of ~0.5 ± 0.2 Myr. These data support a key conclusion: cooling rates at million-year timescales

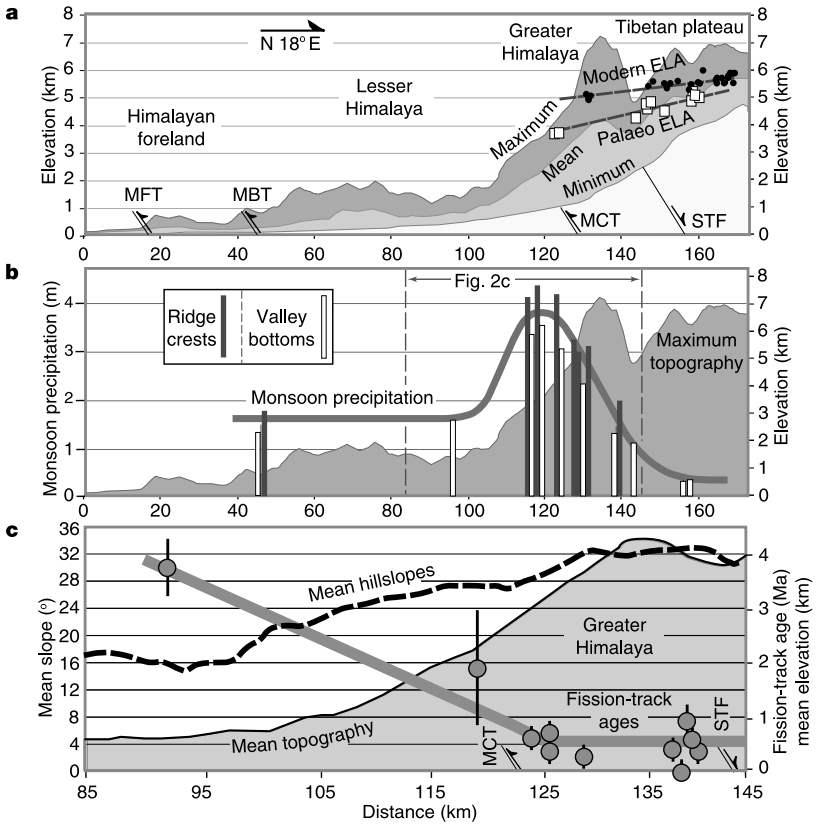


**Figure 2** Monsoon precipitation, apatite fission-track ages, glacial equilibrium-line altitude (ELA) and topographic characteristics of the Marsyandi drainage. MFT, Main Frontal thrust. **a**, Maximum, minimum, and mean elevation within a 50-km-wide swath oriented parallel to the strike of the range in the study area. Major faults (STF, MCT, MBT and MFT) are shown. Modern (black circles) and glacial-era (white squares) equilibrium-line altitudes define northward-rising gradients with a steeper gradient during glacial times. **b**, Monsoon precipitation projected against maximum topography through the study area. Monsoon rainfall is ~10-fold greater on the southern Himalayan flank than north of the Annapurna crest. The spatial extent of **c** is indicated. **c**, Apatite fission-track ages plotted against mean topography. Between the MCT I and the STF system, the apatite fission-track ages are consistently very young (<1 Myr). No apparent gradient in ages exists across the Greater Himalaya. Mean hillslope angles systematically increase northward across the zone of uniform cooling ages.

across the Greater Himalaya are rapid and spatially invariant.

These apatite fission-track dates are as young as, or younger than, apatite fission-track dates reported for Nanga Parbat[14] and the Southern Alps of New Zealand[15], where denudation is interpreted to exceed 4 mm $yr^{-1}$. Although the Marsyandi samples come from valley bottoms where isotherms should be most compressed, observed cooling rates across the Greater Himalaya of ~300 °C $Myr^{-1}$ are, nonetheless, consistent with long-term erosion rates of ≥2–5 mm $yr^{-1}$.

The abrupt increase in cooling rates at the northern edge of the Lesser Himalaya coincides spatially with a doubling of monsoon precipitation (Fig. 2b) due to the orographic effects of Greater Himalayan topography. Such correlations appear consistent with the hypothesis of a coupling between precipitation, channel gradients, and erosion rates. In contrast, the absence of a trend in apatite fission-track ages across the Greater Himalaya, despite at least a fivefold change in precipitation across this same area (Fig. 2b and c), indicates that no direct precipitation–erosion linkage exists across this area.

Alternative interpretations might explain spatially invariant cooling/erosion rates. In contrast to the present, average Pleistocene rainfall could have had a weaker gradient across the range. During the past 1 Myr, climatic variations have been primarily due to glacial–interglacial fluctuations. In the absence of direct measures of past precipitation, the equilibrium-line altitude of glaciers can serve as a proxy for precipitation changes[16]. Whereas the regional gradient of modern equilibrium-line altitudes in the Marsyandi catchment exhibits a northward-rising slope of ~17 m $km^{-1}$, the gradient more than doubled to >36 m $km^{-1}$ during glacial times (Fig. 2a), suggesting amplification of the regional rainfall gradient during glacial times. Thus, relative to the southern Himalayan flank, the northern half of the Marsyandi catchment should have been drier during glaciations than at present. Such conditions appear even more contradictory to a direct precipitation–erosion rate linkage.

A high geothermal gradient due to fluxes of hydrothermal water towards valley bottoms could create apatite fission-track dates that are younger than expected for any given erosion rate[17]. Indeed, numerous hot springs occur along the Marsyandi transect. Apatite fission-track dates from ridge crests (Table 1), however, indicate rapid cooling rates (>100 °C $Myr^{-1}$) at sites up to 2 km above the valley bottom, thereby supporting the conclusion of rapid erosion, irrespective of the role of hydrothermal fluids. Moreover, the spatial uniformity of young apatite fission-track dates along the Marsyandi in the Greater Himalaya, rather than the absolute erosion rate, is central to our interpretation. Neither alternative interpretation offers a viable explanation for the observed uniformity in cooling rates.

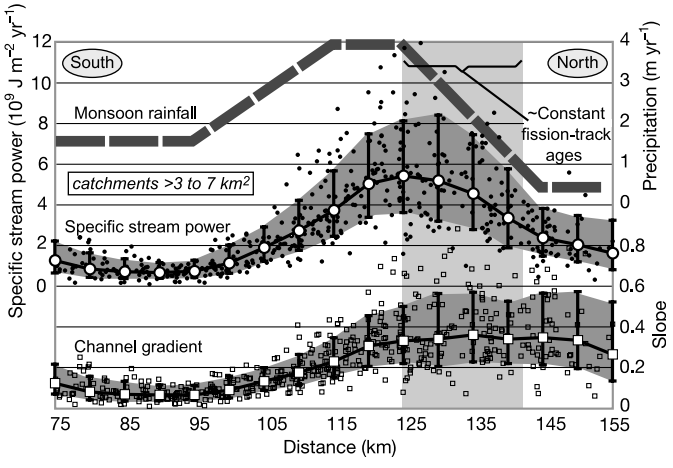


**Figure 3** Plot of channel gradients, specific stream power, and precipitation gradient versus distance for Marsyandi tributary catchments ranging from 3 to 7 $km^2$. The vertical grey swath indicates the zone in which fission-track ages average ~0.5 Myr and uniform, rapid erosion rates are inferred. Note that, although hillslope angles continue to steepen across this zone (Fig. 2c), channel slopes may have attained a threshold gradient (~0.35) in this same region. Whereas rainfall diminishes ~80% across this region, specific stream power only decreases 45% because narrower channels in drier areas focus the available stream power on a smaller channel perimeter.

Mechanisms by which spatially uniform erosion is maintained across the Greater Himalaya, despite greatly decreased precipitation, can be inferred from the digital topography and glacial history of the region. Although the extent of Late Pleistocene glaciation in the Marsyandi is debated[18,19], glacial sculpting of the landscape is unmistakable. Glaciers have the potential to erode at rates ≥5 mm $yr^{-1}$ (ref. 20); such rates would be sufficient to generate erosion rates in the glaciated upper Marsyandi equivalent to fluvial incision rates on the southern Himalayan flank, despite lower precipitation in the north.

In non-glaciated parts of the landscape, systematic topographic changes suggest how spatially uniform erosion rates are sustained for both hill slopes and river channels. First, as precipitation decreases northward from the MCT (Fig. 2b), mean hillslope angles increase (Fig. 2c), despite roughly uniform bedrock strength within the Greater Himalayan crystalline rocks[21]. Such steepening is consistent with hill slopes staying near the threshold for failure by bedrock landslides[22], where higher pore pressures promote landsliding: steeper slopes compensate lower pore pressures in drier areas. Second, river channels could also become steeper to offset decreasing rainfall. Within the Greater Himalaya, however, channel gradients are already steep (~0.35) and do not increase northward (Fig. 3). Nonetheless, assuming that width scales with discharge, $Q$, as $Q^{0.4}$, specific stream power decreases only ~45% across the Greater Himalaya, despite an 80% drop in rainfall. Thus, to the extent that erosion rates scale with specific stream power[23], narrower channels offset about half of the decrease in precipitation. Third, if hillslope erosion is spatially uniform, then more northerly rivers should have higher sediment concentrations. Because most Himalayan rivers have excess sediment-transport capacity, higher sediment concentrations should enhance the frequency of clasts hitting the bed, thereby augmenting erosion rates[24] in drier areas. Thus, steeper hill slopes, narrower rivers, higher sediment concentrations, and efficiently eroding glaciers could yield spatially uniform erosion, despite decreasing precipitation and constant channel slopes.

These new Himalayan data do not, however, explain why hill slopes steepen or uniform erosion exists within the Greater Himalaya, but not elsewhere (Fig. 2). Precipitation clearly is not the dominant control. Instead, we suggest that convergence between India and southern Tibet (~18 mm $yr^{-1}$; ref. 25) has caused persistent lateral and vertical transport of rock into the orogen. When sustained for several million years, the resultant orogen should evolve toward flux and topographic steady states, in which erosional effluxes balance the tectonic influx[26], while crustal thickness and mean topography remain temporally constant. A north-dipping, crustal-scale ramp is proposed to lie beneath the Greater Himalaya[27,28], where its dip angle and associated slip rate should dictate upward particle velocities, with respect to the geoid, in the overthrusting plate. A planar ramp[7,27,28] could predict ramp-parallel transport of rocks at a uniform rate. When balanced by erosion, this prediction is consistent with the observed zone of uniform fission-track ages. We conclude, therefore, that Indo-Tibetan convergence combines with the geometry of overthrusting to strongly influence patterns of erosion across the Greater Himalaya. The shape of the landscape itself results from an interplay of surface processes with precipitation gradients such that erosion is sufficient to balance tectonic deformation. □

## Methods

### Meteorology

A network of 14 meteorological stations was installed across the Annapurna range before the 1999 monsoon season, and expanded to 19 stations encompassing 28 rain gauges in 2000. Rainfall is totalled every 30 min. 'Look-down' distance rangers and $\gamma$-ray loggers measure snow depth and total water content, respectively, once a day at high elevations (>2,500 m in the Greater Himalaya). Only liquid precipitation is measured in the Tibetan zone, such that the annual (but not the monsoon) total is underestimated here. The data presented here (Fig. 2b) represent monsoon averages based on the longest record available from each station.

### Apatite fission-track dating

Following mineral separation, apatites were polished, etched and irradiated. Standard and induced track densities were determined on Brazil ruby muscovite external detectors (geometry factor 0.5), and fossil track densities were determined on internal mineral surfaces. Ages were calculated using $\zeta = 359 \pm 20$ for dosimeter glass CN-5. All ages are central ages and are reported with 1$\sigma$ errors. Long-term erosion rates are conservatively estimated on the basis of the fission-track age, and assuming a geothermal gradient of 100 °C km$^{-1}$ and an annealing temperature of 140 °C.

### Topographic analysis

A 3-arcsec (~90 m) digital elevation model (DEM) is the basis of all topographic analyses. Hillslope angles are calculated at every pixel in the DEM based on a 3 × 3 pixel (~180 × 180 m) grid. Mean hillslope angles were extracted from a moving, 5-km-radius window centred on the Marsyandi River. Maximum, minimum and mean elevation (Fig. 2) were calculated along a 50-km-wide swath oriented perpendicular to the strike of the range and centred on the Marsyandi River (or the Nar-Phu River above its confluence with the Marsyandi).

### Equilibrium-line altitude

Glacial areas were calculated from present and reconstructed ice margins mapped on aerial photographs, and transferred first to 1:50,000 scale topographic maps and then to the digital topography. Based on glacial hypsometry, equilibrium-line altitudes were estimated with an assumed accumulation-area ratio of 0.65. To avoid uncertainty introduced by avalanches on to glaciers from adjacent high peaks, 29 small glaciers (95% are <2.5 km$^2$), lacking high headwalls, were analysed. The regional equilibrium-line altitude gradient shows little sensitivity to accumulation-area ratios ranging from 0.4 to 0.8.

### Specific stream power

Analysis was focused on catchments ranging from 3 to 7 km$^2$ within the non-glaciated part (<4,200 m elevation) of the study area. These basins drain approximately half of the landscape and are sufficiently large to be fluvial, as opposed to colluvial/debris flow, channels. Monsoon rainfall was smoothed across the meteorological network to define an average precipitation gradient perpendicular to the strike of the topography. This gradient was then extrapolated parallel to strike across the study area. For each river segment ≥500 m long, channel gradients ($S$) were extracted from the DEM, and discharge ($Q$) was calculated as the product of upstream area and rainfall. Discharge is overestimated because all rainfall is assumed to enter channels. Channel width ($W$) is calculated as $10^{-2}\,Q^{0.4}$. Specific stream power (in GJ m$^{-2}$ yr$^{-1}$) is calculated as $\rho_w g QS/W$, where $\rho_w$ is the density of water and $g$ is gravitational acceleration. Channel gradients and specific stream power are binned every 5 km.

Received 20 June; accepted 4 November 2003; doi:10.1038/nature02187.


1. Koons, P. O. The topographic evolution of collisional mountain belts: A numerical look at the Southern Alps, New Zealand. *Am. J. Sci.* **289,** 1041–1069 (1989).
2. Beaumont, C., Jamieson, R. A., Nguyen, M. H. & Lee, B. Himalayan tectonics explained by extrusion of a low-viscosity crustal channel coupled to focused surface denudation. *Nature* **414,** 738–742 (2001).
3. Willett, S. D. Orogeny and orography: The effects of erosion on the structure of mountain belts. *J. Geophys. Res.* **104,** 28957–28982 (1999).
4. Hodges, K. V. Tectonics of the Himalaya and southern Tibet from two perspectives. *Geol. Soc. Am. Bull.* **112,** 324–350 (2000).
5. Tapponnier, P. *et al.* Oblique stepwise rise and growth of the Tibetan Plateau. *Science* **394,** 1671–1677 (2001).
6. Burchfiel, B. D. *et al.* The South Tibetan detachment system, Himalayan orogen: Extension contemporaneous with and parallel to shortening in a collisional mountain belt. *Geol. Soc. Am. Spec. Pap.* **269,** 1–41 (1992).
7. Harrison, T. M. *et al.* A late Miocene-Pliocene origin for the central Himalayan inverted metamorphism. *Earth Planet. Sci. Lett.* **146,** E1–E7 (1997).
8. Catlos, E. J. *et al.* Geochronologic and thermobarometric constraints on the evolution of the Main Central Thrust, central Nepal Himalaya. *J. Geophys. Res.* **106,** 16177–16204 (2001).
9. Robinson, D. M. *et al.* Kinematic model for the Main Central thrust in Nepal. *Geology* **31,** 359–362 (2003).
10. Hurtado, J. M. Jr, Hodges, K. V. & Whipple, K. Neotectonics of the Thakkhola Graben and implications for Recent activity on the South Tibetan fault system in the central Nepal Himalaya. *Geol. Soc. Am. Bull.* **113,** 222–240 (2001).
11. Dodson, M. H. in *Lectures in Isotope Geology* (eds Jaeger, E. & Hunziker, C. J.) 194–202 (Springer, New York, 1979).
12. Stüwe, K., White, L. & Brown, R. The influence of eroding topography on steady-state isotherms. Application to fission track analysis. *Earth Planet. Sci. Lett.* **124,** 63–74 (1994).
13. Willett, S. D. & Brandon, M. T. On steady states in mountain belts. *Geology* **30,** 175–178 (2002).
14. Zeitler, P. K. Cooling history of the NW Himalaya, Pakistan. *Tectonics* **4,** 127–151 (1985).
15. Tippett, J. M. & Kamp, P. J. J. Fission track analysis of the Late Cenozoic vertical kinematics of continental Pacific crust, South Island, New Zealand. *J. Geophys. Res.* **98,** 16119–16148 (1993).
16. Porter, S. C. Some geological implication of average Quaternary glacial conditions. *Quat. Res.* **32,** 245–261 (1989).
17. Ehlers, T. A., Armstrong, P. A. & Chapman, D. S. Normal fault thermal regimes and the interpretation of low-temperature thermochronometers. *Phys. Earth Planet. Inter.* **126,** 179–194 (2001).
18. Fort, M. B. Glacial extension and catastrophic dynamics along the Annapurna Front, Nepal Himalaya. *Göttinger Geogr. Abh.* **81,** 105–121 (1986).
19. Duncan, C. C., Klein, A. J., Masek, J. G. & Isacks, B. L. Comparison of Late Pleistocene and modern glacier extents in central Nepal based on digital elevation data and satellite imagery. *Quat. Res.* **49,** 241–254 (1998).
20. Hallet, B., Hunter, L. & Bogen, J. Rates of erosion and sediment evacuation by glaciers: A review of field data and their implications. *Glob. Planet. Change* **12,** 213–235 (1996).
21. Hodges, K. V., Parrish, R. R. & Searle, M. P. Tectonic evolution of the central Annapurna Range, Nepalese Himalayas. *Tectonics* **15,** 1264–1291 (1996).
22. Burbank, D. W. *et al.* Bedrock incision, rock uplift, and threshold hillslopes in the northwestern Himalaya. *Nature* **379,** 505–510 (1996).
23. Whipple, K. E., Kirby, E. & Brocklehurst, S. H. Geomorphic limits to climate-induced increases in topographic relief. *Nature* **401,** 39–43 (1999).
24. Sklar, L. & Dietrich, W. E. Sediment supply, grain size and rock strength controls on rates of river incision into bedrock. *Geology* **29,** 1087–1090 (2001).
25. Wang, Q. *et al.* Present-day crustal deformation in China constrained by Global Positioning System measurements. *Science* **294,** 574–577 (2001).
26. Willett, S. D., Slingerland, R. & Hovius, N. Uplift, shortening, and steady state topography in active mountain belts. *Am. J. Sci.* **301,** 455–485 (2001).
27. Seeber, L. & Gornitz, V. River profiles along the Himalayan arc as indicators of active tectonics. *Tectonophysics* **92,** 335–367 (1983).
28. Pandey, M. R., Tandukar, R. P., Avouac, J. P., Lave, J. & Massot, J. P. Interseismic strain accumulation on the Himalayan crustal ramp (Nepal). *Geophys. Res. Lett.* **22,** 751–754 (1995).


**Acknowledgements** This work benefited from discussions with K. Hodges, J. Lavé, A. Heimsath, K. Whipple, P. Koons, M. Brandon and T. Ehlers. We thank P. Molnar and C. Beaumont for comments and suggestions. Logistical support from Himalayan Experience and the Nepalese Department of Hydrology and Meteorology is gratefully acknowledged. This work was funded by the NSF Continental Dynamics program and by NASA.

**Competing interests statement** The authors declare that they have no competing financial interests.

**Correspondence** and requests for materials should be addressed to D.W.B. (burbank@crustal.ucsb.edu).

# Undesirable evolutionary consequences of trophy hunting

**David W. Coltman[1], Paul O'Donoghue[1], Jon T. Jorgenson[2], John T. Hogg[3], Curtis Strobeck[4] & Marco Festa-Bianchet[5]**

[1]*Department of Animal and Plant Sciences, University of Sheffield, Sheffield S10 2TN, UK*
[2]*Alberta Department of Sustainable Development, Fish and Wildlife Division, Box 1059, Canmore, Alberta T0L 0M0, Canada*
[3]*Montana Conservation Science Institute, Missoula, Montana 59803, USA*
[4]*Department of Biological Sciences, University of Alberta, Edmonton, Alberta T6G 2E9, Canada*
[5]*Département de biologie, Université de Sherbrooke, Sherbrooke, Québec J1K 2R1, Canada*

**Phenotype-based selective harvests, including trophy hunting, can have important implications for sustainable wildlife management if they target heritable traits[1–3]. Here we show that in an evolutionary response to sport hunting of bighorn trophy rams (*Ovis canadensis*) body weight and horn size have declined significantly over time. We used quantitative genetic analyses, based on a partly genetically reconstructed pedigree from a 30-year study of a wild population in which trophy hunting targeted rams with rapidly growing horns[4], to explore the evolutionary response to hunter selection on ram weight and horn size. Both traits were highly heritable, and trophy-harvested rams were of significantly higher genetic 'breeding value' for weight and horn size than rams that were not harvested. Rams of**